THE CONVECTIVE PRECIPITATION EXPERIMENT (COPE)

Investigating the Origins of Heavy Precipitation in the Southwestern United Kingdom

BY DAVID C. LEON, JEFFREY R. FRENCH, SONIA LASHER-TRAPP, ALAN M. BLYTH, STEVEN J. ABEL, SUSAN BALLARD, ANDREW BARRETT, LINDSAY J. BENNETT, KEITH BOWER, BARBARA BROOKS, PHIL BROWN, CRISTINA CHARLTON-PEREZ, THOMAS CHOULARTON, PETER CLARK, CHRIS COLLIER, JONATHAN CROSIER, ZHIQIANG CUI, SEONAID DEY, DAVID DUFTON, CHLOE EAGLE, MICHAEL J. FLYNN, MARTIN GALLAGHER, CAROL HALLIWELL, KIRSTY HANLEY, LEE HAWKNESS-SMITH, YAHUI HUANG, GRAEME KELLY, MALCOLM KITCHEN, ALEXEI KOROLEV, HUMPHREY LEAN, ZIXIA LIU, JOHN MARSHAM, DANIEL MOSER, JOHN NICOL, EMILY G. NORTON, DAVID PLUMMER, JEREMY PRICE, HUGO RICKETTS, NIGEL ROBERTS, PHIL D. ROSENBERG, DAVID SIMONIN, JONATHAN W. TAYLOR, ROBERT WARREN, PAUL I. WILLIAMS, AND GILLIAN YOUNG

A recent field campaign in southwest England used numerical modeling integrated with aircraft and radar observations to investigate the dynamic and microphysical interactions that can result in heavy convective precipitation.

One of the many challenges of improving quantitative precipitation forecasts (QPFs) for summertime convection is achieving a better understanding of cloud microphysics, turbulent entrainment, and boundary layer processes (Fritsch and Carbone 2004). The urgency of this challenge has not been reduced by the increased use of ensembles and convective-permitting ensemble forecast systems in probabilistic forecasting of convection; their improvement also depends upon an enhanced understanding of physical processes applied to the constituent deterministic models (Fritsch and Carbone 2004).

Flash flooding is an issue worldwide: some of the world's most destructive flash floods occur in the Indian monsoon. For example, severe flooding occurred in Ladakh, India, on 6 August 2010 as a result of extremely heavy rain believed to have peaked at about 150 mm h^{-1} (e.g., Kumar et al. 2014). There are, however, many examples of flash floods at midlatitudes as well. Some in the United States include Jamestown, Pennsylvania, in 1889 and 1977; Big Thompson, Colorado, in 1976; Rapid City, South Dakota, in 1972; Ft. Collins, Colorado, in 1997; and in Boulder, Colorado, in 2013. The important elements for flash flooding include intensity, duration, and location of the rainfall. On 16 August 2004 high humidity in the troposphere, combined with a stationary convergence line, led to the development of deep convective clouds that produced intense rain over a period of about 4 h, with up to 183 mm of precipitation recorded over a 5-h period, resulting in flash flooding in the village of Boscastle in southwest England (Golding et al. 2005).

Warm rain, precipitation produced solely through condensation and accretion of liquid, is known to be important in the tropics (e.g., Rogers 1967; Houze 1977). However, the warm rain process may also play a critical role in heavy convective precipitation events in midlatitudes as well; many of the flash floods cited above are examples (Caracena et al. 1979; Petersen et al. 1999; Pontrelli et al. 1999; Golding et al. 2005; etc.). Heavy rain produced exclusively through warm processes was observed in the southwest of England during the field campaign discussed in this paper.

Supercooled raindrops originating from the warm rain process have long been known to play a role in the precipitation process in convective clouds (e.g., Koenig 1963; Jameson et al. 1996; Kumjian and Ryzhkov 2008). Upon freezing, these drops are converted to graupel via riming and can lead to the formation of secondary ice splinters, thereby accelerating ice production in the cloud. Details are not known of the rate of production of embryos—cloud droplets >20-μm diameter that can grow by accretion—leading to an effective warm rain process, the nucleation of ice particles, and the rate of production of secondary ice particles by the Hallett–Mossop process. Furthermore, the interaction between microphysics and dynamics and the details of how certain processes operate remain uncertain.

Recent major developments in operational numerical weather prediction (NWP) models include the use of high-resolution convective-scale models, such as the 1.5-km Unified Model (UM) used by the Met Office (UKMO) and the 3-km High-Resolution Rapid Refresh model used by the U.S. National Weather Service. Such models aim to deliver improved forecasts of convection and are much more realistic and skillful than coarser-resolution models (e.g., Roberts and Lean 2008). However, deterministic forecasts of convective systems are limited, and probabilistic convection-permitting ensemble forecasts are becoming possible and more reliable (e.g., Clark et al. 2009; Dey et al. 2014). Both cloud-permitting deterministic and probabilistic models would benefit from improved knowledge and representation of key microphysical processes and their rates (Duda et al. 2014).

Recently, three related projects designed to investigate convective initiation were conducted: the International H_2O Project (IHOP_2002) in the Great Plains of the United States (Weckwerth et al. 2004), the Convective Storm Initiation Project (CSIP) in the maritime conditions of southern England (Browning et al. 2007), and the Convective and Orographically-Induced Precipitation Study (COPS) in the Black Forest mountains in southwest (SW) Germany and Vosges mountains in southeast France (Wulfmeyer et al. 2011). Significant progress was made in each in terms of understanding some of the phenomena responsible for the initiation and development of convective clouds. The Convective Precipitation Experiment (COPE), in contrast to these projects, investigated the entire life cycle of convection, emphasizing the interaction of dynamics and microphysics using a combination of in situ and radar measurements together with high-resolution model studies.

COPE was designed to study the complete storm evolution, including the details of convergence lines, storm growth and persistence, and the microphysics

AFFILIATIONS: Leon, French, and Plummer—Department of Atmospheric Science, University of Wyoming, Laramie, Wyoming; Lasher-Trapp and Moser—Department of Atmospheric Sciences, University of Illinois at Urbana–Champaign, Urbana, Illinois; Blyth, Bennett, Brooks, Collier, Dufton, and Marsham—National Centre for Atmospheric Science, School of Earth and Environment, University of Leeds, Leeds, United Kingdom; Abel and Brown—Met Office, Exeter, United Kingdom; Ballard, Charlton-Perez, Choularton, Dey, Eagle, Halliwell, Hanley, Hawkness-Smith, Kelly, Lean, Roberts, and Simonin—Met Office@Reading, University of Reading, Reading, United Kingdom; Barrett—Department of Meteorology, University of Reading, Reading, United Kingdom; Bower, Cui, Flynn, Gallagher, Kitchen, Liu, Taylor, and Young—School of Earth, Atmospheric and Environmental Sciences, University of Manchester, Manchester, United Kingdom; Clark—Met Office, and Department of Meteorology, University of Reading, Reading, United Kingdom; Crosier, Norton, Ricketts, and Williams—National Centre for Atmospheric Science, School of Earth, Atmospheric and Environmental Sciences, University of Manchester, Manchester, United Kingdom; Korolev—Cloud Physics and Severe Weather Research Section, Environment and Climate Change Canada, Toronto, Ontario, Canada; Huang and Rosenberg—School of Earth and Environment, University of Leeds, Leeds, United Kingdom; Nicol—National Centre for Atmospheric Science, Department of Meteorology, University of Reading, Reading, United Kingdom; Price—Meteorological Research Unit, Met Office, Cardington, United Kingdom; Warren—School of Earth, Atmosphere, and Environment, Monash University, Melbourne, Victoria, Australia
CORRESPONDING AUTHOR: Dr. David Leon, Dept. of Atmospheric Science, University of Wyoming, Engineering Bldg. 6045, 1000 E. University Ave., Laramie, WY 82071
E-mail: leon@uwyo.edu

The abstract for this article can be found in this issue, following the table of contents.

DOI:10.1175/BAMS-D-14-00157.1

A supplement to this article is available online (10.1175/BAMS-D-14-00157.2)

In final form 28 July 2015

of cloud and precipitation over the southwestern peninsula of the United Kingdom. COPE, with its emphasis on the comparison of observations with high-resolution numerical simulations, complements results from the recent Dynamical and Microphysical Evolution of Convective Storms (DYMECS) experiment, which also took place over the southwestern United Kingdom but used a statistical approach, comparing radar data from 40 days of convective storms to simulated storm structures at horizontal grid spacing ranging from 1.5 km to 100 m (Stein et al. 2015).

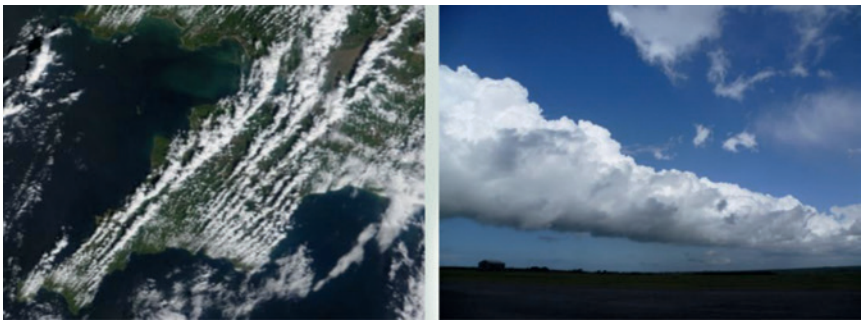

Fig. 1. Clouds tend to form along convergence lines in the southwest peninsula of England when the wind is from the SW. Cloud streets also form, but it is the convergence lines formed by sea-breeze fronts where the strongest clouds tend to develop. (left) An image from the *Terra* satellite; (right) a photo of the clouds that developed significantly. Both images are from 2 Aug 2013.

Key advantages of the COPE study area include its small geographical domain and the frequency of clouds forming along convergence lines (e.g., Morcrette et al. 2007; Lean et al. 2009) as can be seen in Fig. 1. Thus, a single location (Davidstow) could be used for major ground-based instruments including the National Centre for Atmospheric Science (NCAS) X-band radar, the NCAS 1290-MHz wind profiler, and a suite of aerosol measurements. Aircraft could avoid drawn-out excursions to sample clouds, and cells at various stages in their life cycle could be sampled by flying along these lines. In southwest England, the shape of the peninsula encourages the formation of convergence lines in the prevailing southwesterly winds, resulting in one or more lines of cumulus congestus. Warren et al. (2014) found that the most likely cause of lines in this area is the merging of sea-breeze fronts formed from differential heating.

COPE incorporated both field observations and a hybrid set of numerical models run at different scales throughout the field experiment in order to i) determine the dominant cloud physical processes in convective rainfall and evaluate the rates of these processes, especially the initiation stages of warm rain and ice processes through intense rainfall, and the interactions between microphysics and dynamics, notably the influence of entrainment and mixing, and the production of downdrafts; ii) understand and evaluate boundary layer processes that lead to the development and persistence of convective clouds; iii) assess and improve the performance of multiple U.K. NWP models in predicting convective clouds and rainfall; and iv) determine and address the dominant sources of uncertainty in the prediction of convective rainfall.

FIELD CAMPAIGN. The COPE field campaign took place during July and August 2013. Most deep convection occurred during a period in late July through early August. Observations were made using three aircraft, ground-based and airborne radars and lidars, aerosol instrumentation, and multiple atmospheric sounding systems. An extensive description of the instruments deployed during COPE is provided in the accompanying electronic supplement (http://dx.doi.org/10.1175/BAMS-D-14-00157.2). A total of 17 intensive observation periods (IOPs) were conducted (Table 1). Of those, roughly one-third included deep convective clouds, with the rest focused on shallower convection with tops below, or not much higher than, 0°C. Clouds outside the COPE domain were also sampled during two IOPs while a further two IOPs collected data to study convergence in the boundary layer.

To aid in daily planning, deterministic forecasts were provided from the Met Office standard operational global and regional models. The global model was run every 6 h with forecasts out to 7 days. The variable-resolution Unified Model for the U.K. region (UKV; Tang et al. 2013) represents convection explicitly and was run eight times a day on a 3-h assimilation cycle out to 36 h to provide U.K.-specific forecasts of convective activity. A third U.K. fixed-resolution convection-allowing model [United Model—Extended (UKX)] downscaled from the global model, run out to 5 days, gave insight into continuity between the global and UKV models. An analogous ensemble forecast system, the Met Office Global and Regional Ensemble Prediction System (MOGREPS), consisted of a global ensemble (MOGREPS-G) with the 12-member, 2.2-km U.K. domain (MOGREPS-UK) convection-permitting ensemble nested within it (Golding et al. 2014).

Output from the global model and MOGREPS-G were used to assess convective potential at time

Table 1. Intensive observation periods for COPE , where N = north and MCS = mesoscale convective system.

Date	Location	Description	NCAS radar/wind profiler[a]	King Air	BAe 146	MOCCA	COPE sondes
4 Jul		Calibration flights and frictional convergence measurements	X	X	X		
5 Jul	SW England	Sea-breeze front, convergence line evolution (boundary layer study)	X		X	X	
10 Jul	NW Wales	Aerosol layers on lidar; shallow convection reaching 0°C		X			
18 Jul	SW England	Deep convective storms	X	X	X	X	X
23 Jul	SW England	Heavy rainfall from MCS	X[b]				
25 Jul	SW England	Convection along convergence line; warm rain only	X[a]	X	X	X	X
27 Jul	Tip of SW England	Small cells aside of MCS in France	X[a]	X			
28 Jul	SW England	Deep convection, multiple spatial organizations	X[a]	X	X		X
29 Jul	SW England	Organized convective line	X[a]	X	X		X
2 Aug	N Cornwall coast	Deep convective cells with heavy rain	X[a]	X			X
3 Aug	SW England	Persistent line; deep cells and heavy rain	X[a]	X	X		X
5 Aug	SW England	Deep convection along line with localized very heavy rain	X				
6 Aug	SW England	Warm cumuli embedded in stratiform layer	X	X			X
7 Aug	NW Wales	Warm clouds and little rain		X			X
14 Aug	SW England	Warm rain study in cloud complexes	X	X			X
15 Aug	SW England	Line of convection in SW flow; largely dissipated prior to flight	X[a]	X			X
17 Aug	SW England	Flights before and after frontal passage; warm elevated convection before; shallow clouds with ice after	X[a]	X			

[a] Also includes ground-based aerosol measurements and ground-based lidar.

[b] Chilbolton radar also recorded data.

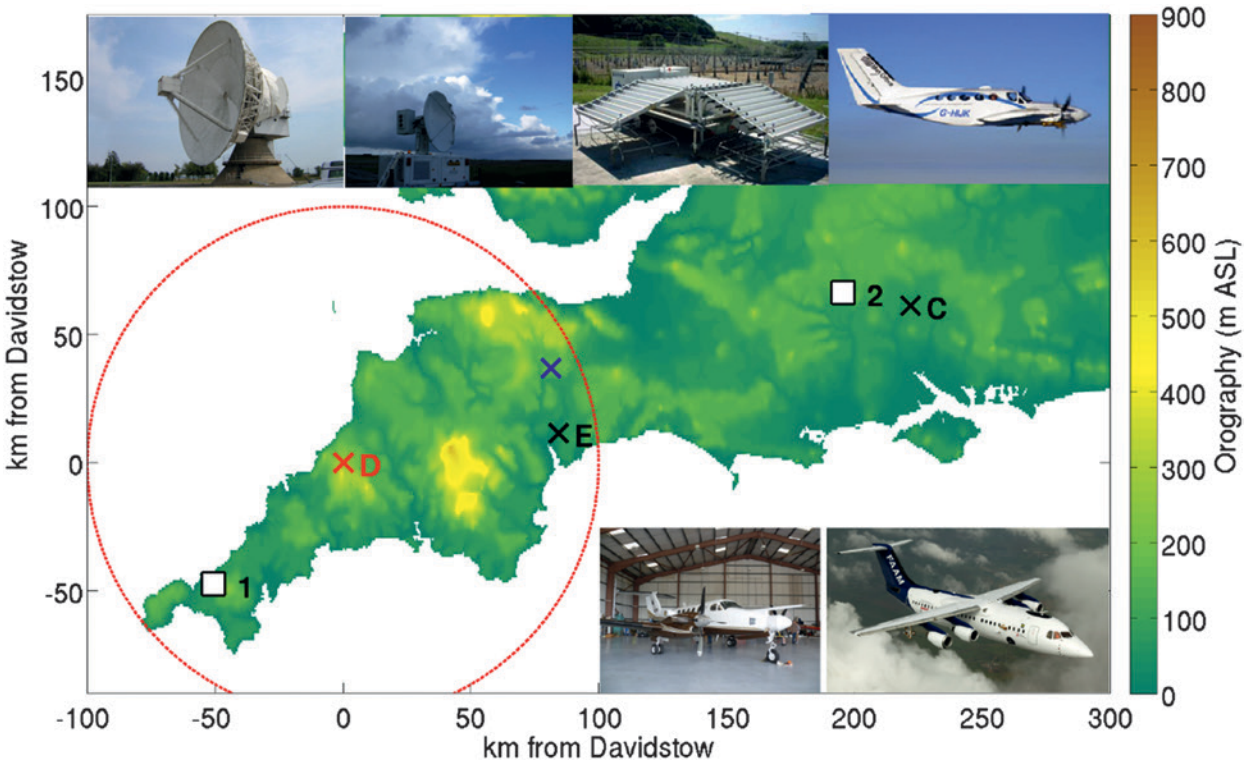

Fig. 2. COPE observing facilities and study area (background). Clockwise from (top left): Chilbolton radar, NCAS X-Band radar, NCAS wind profiler, MOCCA aircraft, BAe 146, and UWKA. Background map: X's show Davidstow at D (X-band radar, 1290-MHz wind profiler), where the dashed circle gives 100-km range from Davidstow; Chilbolton observatory at C; and Exeter at E (base of operations for UWKA and BAe 146). Blue X indicates operational network radar at Cobbacombe Cross. White squares: location of regular sounding launches: 1, Camborne; 2, Larkhill.

scales beyond a few days. The UKX provided convective-scale guidance for 2–5 days, whereas the UKV was most useful for day-of operations and next-day planning. Key products produced by the U.K. models included soundings at selected locations and time–height plots of thermodynamic fields to evaluate the evolution of the vertical structure of the atmosphere prior to and during convection. UKV plan-view maps provided estimates of rainfall, cloud, and low-level convergence important for flight planning.

Operations for COPE were focused over the west-central region of the southwestern peninsula of the United Kingdom, centered on Davidstow (see Fig. 2). General atmospheric thermodynamic and dynamic structures were provided by rawinsondes launched from Davidstow at 1–2-h intervals during IOPs and a collocated 1290-MHz radar wind profiler. These measurements were augmented by Met Office soundings from Camborne and Larkhill released every 12 h throughout the campaign and at frequencies up to 1 h^{-1} during IOPs. Ground-based aerosol observations at Davidstow included size-resolved concentration and aerosol composition and optical properties.

Measurements from the dual-polarization NCAS X-band radar at Davidstow provided spatial context, information about the temporal evolution of convective cells, and an estimation of the precipitation rate near the surface. The X-band radar completed a volume scan approximately every 5 min, providing measures of reflectivity, Doppler velocity, differential reflectivity (Z_{DR}), specific differential phase (K_{DP}), and correlation coefficient (ρ_{hv}). The S-band ground-based radar at Chilbolton collected data during several IOPs and the U.K. network radar at Cobbacombe Cross was operated throughout the campaign, both providing additional measurements for larger storm systems and storms in the far eastern portion of the COPE domain.

During operations, coordination between the aircraft and observing facilities on the ground was critical to focus sampling on clouds within the same region using real-time radar measurements from the NCAS X-band radar to identify regions of interest. Airborne sampling during the early stages of IOPs focused on the prestorm environment. Measurements from the Met Office Civil Contingency Aircraft (MOCCA) and the U.K. Facility for Airborne Atmospheric Measurements (FAAM) BAe 146

provided detailed information on aerosol, winds, and thermodynamics in the preconvective boundary layer. As part of the prestorm sampling, the BAe 146 flew two legs, one along and another across the peninsula, timed such that the end of the legs coincided with the forecast initiation of deeper convection and the arrival of the University of Wyoming King Air (UWKA).

Together, the BAe 146 (Petersen and Renfrew 2009; Allen et al. 2011; Cotton et al. 2013) and the UWKA (Rodi 2011) focused on sampling clouds in the same region. For missions where both aircraft were available, the BAe 146 initially made penetrations at cloud base and the UWKA penetrated clouds as their tops ascended through the 0°C level. As the clouds grew deeper, both aircraft stepped higher, with the UWKA remaining above the BAe 146. In all cases, the aircraft focused penetrations near the tops of growing turrets as they ascended through flight level. Instruments on both the BAe 146 and the UWKA provided measurements of cloud dynamical and microphysical parameters and thermodynamic variables. Multiple instruments provided independent estimates of liquid water content (LWC) at scales down to tens of meters. Particle size distributions were measured for particles ranging from a few micrometers to several millimeters in diameter. On the BAe 146, probes with overlapping size ranges allowed direct comparison between concentrations measured by the different probes. Shape-based particle phase determination was applied to optical array probe (OAP) measurements from both aircraft.

Airborne radar observations made with the Wyoming Cloud Radar (WCR), a 95-GHz dual-channel Doppler radar on board the UWKA, provided high-resolution context for the clouds being sampled. The WCR measured profiles of reflectivity and Doppler velocity in a near-vertical curtain defined by the UWKA aircraft track at resolutions of tens of meters. The WCR signal is attenuated by cloud water and even more strongly by raindrops. The strong attenuation in high rainwater conditions limits the penetration depth of the signal into cloud but also provides a robust indicator of a vigorous warm rain process (e.g., Lhermitte 1990). This has proven useful for interpreting detailed measurements from the in situ microphysics probes on both aircraft.

Observations from the airborne Wyoming Cloud Lidar (WCL; Wang et al. 2012) provided accurate determination of cloud-top heights and eddy characteristics for flight legs above cloud top. The WCL is a downward-looking 355-nm elastic backscatter lidar with a resolution of a few meters in the vertical. In addition to measuring cloud-top height, the WCL can also detect the top of the boundary layer and the presence

AEROSOL LAYERS OVER CONVECTIVE CLOUDS ON 10 JULY

Aerosol layers overlying a field of growing cumulus sampled over Wales on 10 July 2013 evident in the WCL attenuated backscatter (uncalibrated). Back trajectories computed using Hybrid Single-Particle Lagrangian Integrated Trajectory model (HYSPLIT) suggest a probable origin for the layers 7 days earlier over northern Africa interspersed with trajectories originating over the North Atlantic giving rise to the finescale layering evident in Fig. SB1 The image shows a transect of about 10 km nearly aligned with the shear. The layers, assumed to be nearly horizontal prior to being displaced by the growing cumulus, provide a dramatic visualization of the interaction of the growing cloud with its environment. Particularly noteworthy is how the layers are drawn significantly downward (by about 500 m) on the downshear side of the cloud with the disturbance extending well above cloud top and nearly half the diameter of the cloud downshear of the turret.

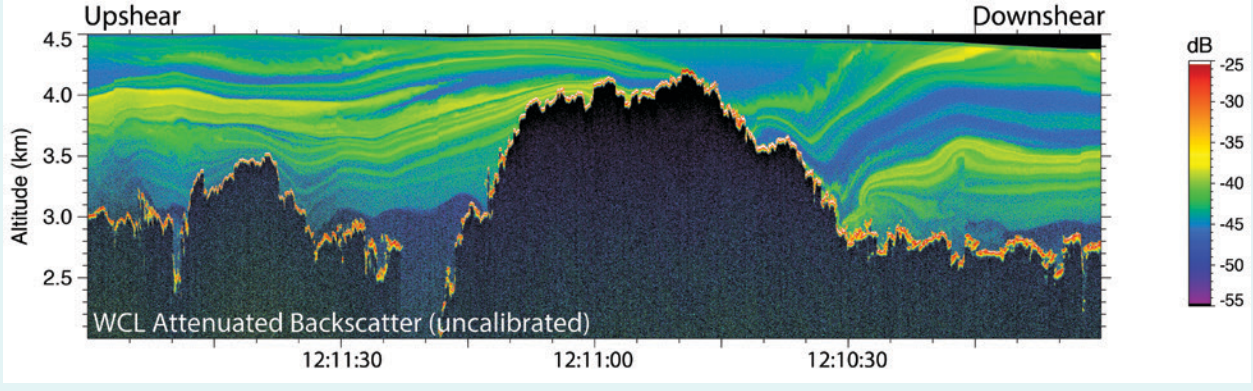

Fig. SB1. Attenuated backscatter from the downward-looking WCL (uncalibrated) showing fine aerosol layers displaced by convection growing into the layer. .

of aerosol layers (see sidebar on aerosol layers over convective clouds on 10 July for more information).

Near the end of each flight, the BAe 146 penetrated clouds near their maximum tops (–10° to –15°C or colder, depending on the day), while the UWKA flew above cloud top observing the clouds with its downward-pointing cloud radar and lidar. Clouds were sampled using a loosely coordinated quasi-statistical approach; no attempt was made to coordinate sampling of individual cells.

Additional details of the ground-based and airborne instruments, operations periods for instruments that were not available for the entire campaign, and significant known instrument and data issues are detailed in the electronic online supplement (http://dx.doi.org/10.1175/BAMS-D-14-00157.2).

COPE HIGHLIGHTS. *The preconvective environment.* Characteristics of the preconvective eenvironment, including the formation and configuration of convergence lines, boundary layer depth, and aerosol concentration, influence the timing and location of convective initiation, the subsequent evolution of convection, and the eventual distribution of precipitation. High-resolution modeling was used to explore the sensitivity of the strength and structure of the convergence lines to model resolution. The numerical simulations were supplemented by observations from the aircraft, NCAS radar, and wind profiler.

The 1.5-km UKV model that was used for routine forecasting in COPE is one of a new generation of kilometer-scale convection-permitting models where the convection is represented explicitly rather than by a convection parameterization (Clark et al. 2016). The representation of convection in the model as a function of decreasing grid spacing down to around 100 m is a subject of research. For the Met Office UM, this work was started as part of the DYMECS project

AEROSOL COMPOSITION ON 3 AUGUST

Aerosol composition measured during below-cloud aerosol runs over Cornwall on 3 August are shown in Fig. SB2. Back trajectories on this day showed the air mass had been over the Atlantic for at least 5 days before moving over the peninsula from the southwest. Sulfate and organic aerosol (OA) were present in similar concentrations inland and off the coast, suggesting they were of marine origin, though the sulfate was in the form of sulfuric acid over the sea and ammonium sulfate inland. The low black carbon (BC) content over land suggests any local fossil fuel emissions can only have had a minor effect; the main anthropogenic influence was the addition of ammonium to neutralize the sulfuric acid. The main source of cloud condensation nuclei (CCN) in this case study appears to be marine sulfate, likely formed by oxidation of dimethyl sulfide (DMS). The majority of supermicron aerosol mass collected on filters was chloride compounds (i.e., sea salt) and around 20% was silicates, which may be a source of ice nuclei.

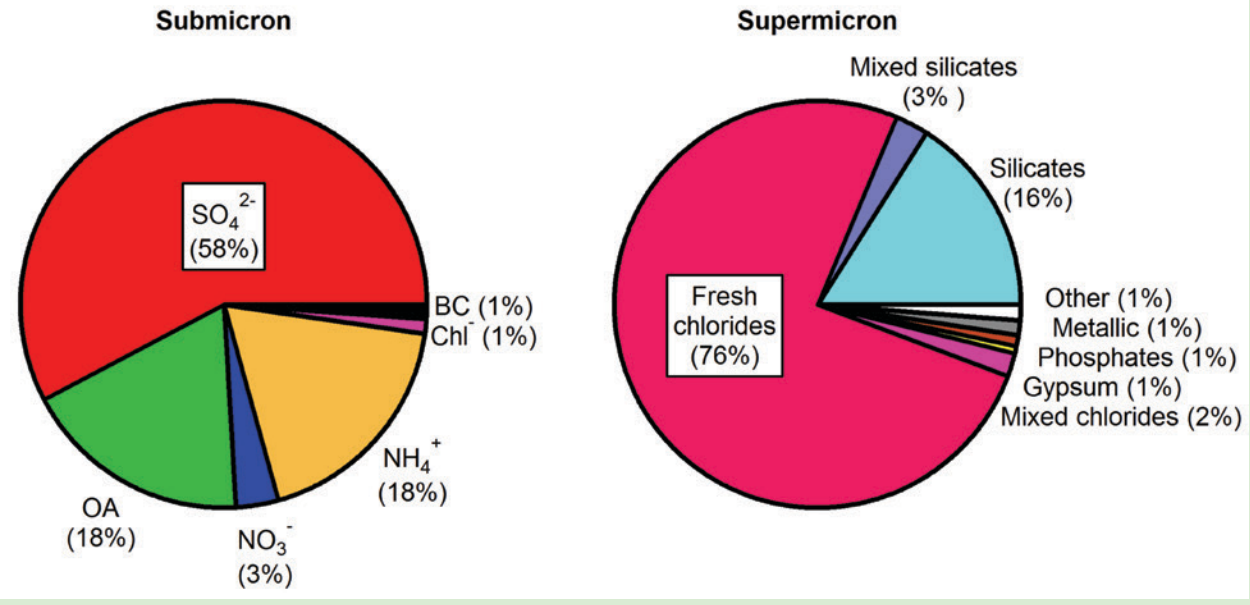

Fig. SB2. Aerosol composition measured with the BAe 146 aircraft during below-cloud aerosol runs over Cornwall on 3 August. The composition of (left) submicron and (right) supermicron aerosols is shown.

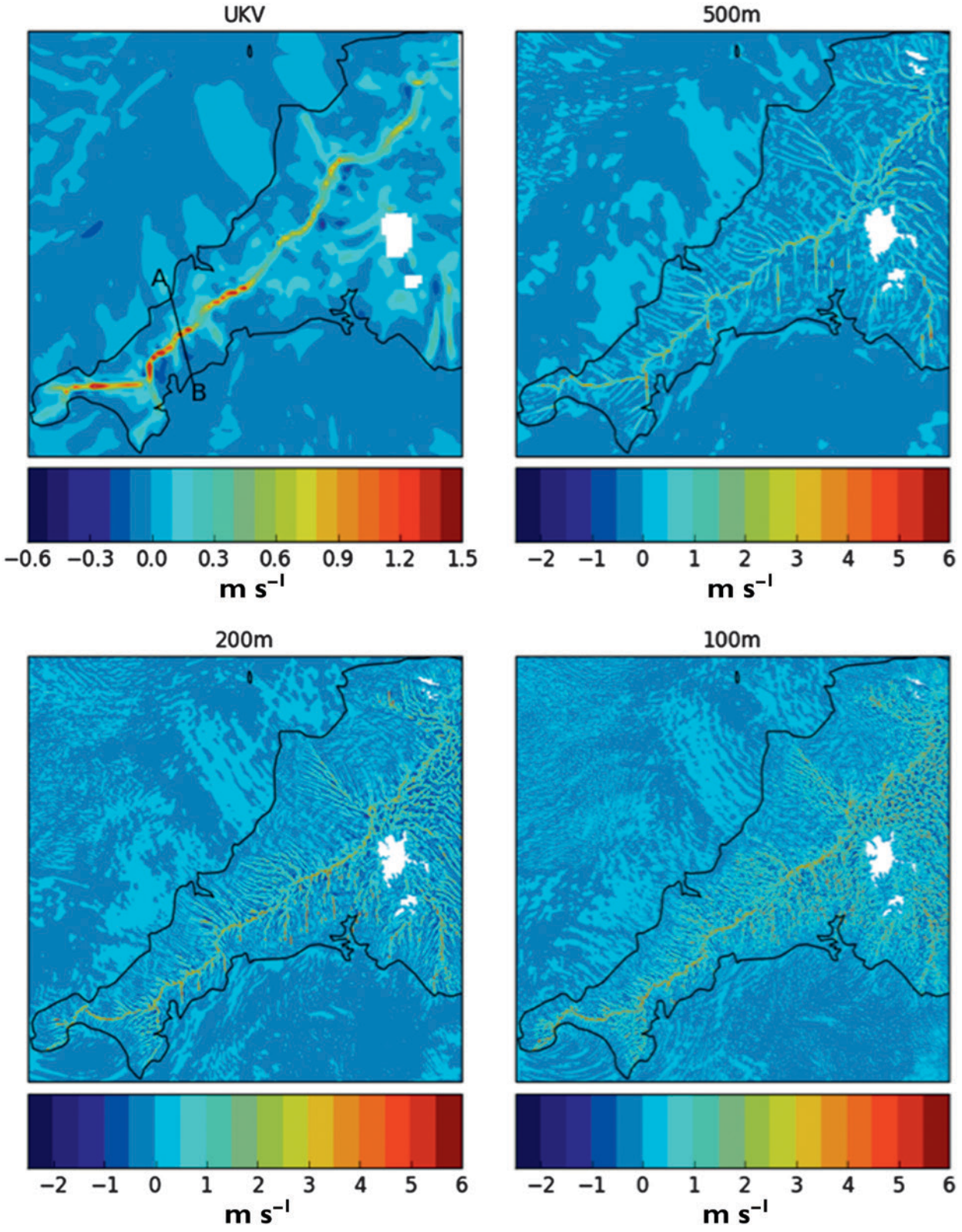

Fig. 3. Vertical velocity at 450 m in models at resolutions ranging from (top left, UKV) 1.5 km down to (bottom right) 100 m at 1315 UTC 5 Jul 2013. (top left) Note smaller velocity scale for UKV. White areas indicate where the terrain height exceeds the 450-m level shown. Line A–B in (top left) indicates location of cross section shown in Fig. 4.

GIANT RAINDROPS SAMPLED ON 2 AUGUST

Giant raindrops! Raindrops exceeding 8 mm in diameter were observed on 2 August at levels as cold as −6°C. Such large raindrops have been observed previously at or below cloud base in tropical clouds (Beard et al. 1986; Hobbs and Rangno 2004) and at midlevels in clouds in the central and southeastern United States (Bringi et al. 1996, 1997). However, these are the first such observations in clouds at such high latitudes and were one of the surprises from COPE. Figure SB3 shows several drops imaged by the 2D precipitation (2DP) OAP on the UWKA as it passed through a single cloud on 2 August. Most of the drops are partial images (yellow background). The first drop in the sequence had a diameter of 8.4 mm.

Fig. SB3. Images of exceptionally large raindrops from an optical array probe (OAP-2DP) onboard the UWKA.

(Stein et al. 2015). COPE allows detailed analysis of well-observed cases of a different nature. After the end of the field phase of the project all the IOPs were rerun with a nested set of UM configurations consisting of a 500-, 200-, and 100-m model nested within the 1.5-km-resolution UKV. This was done in order to provide baseline results to serve as a basis for future more detailed work on different cases. The model configurations used were as in the DYMECS project (Hanley et al. 2015)—the main significant change in the 500-m and finer models being the use of a 3D Smagorinsky mixing scheme, rather than a 2D Smagorinsky horizontal scheme and a separate boundary layer scheme in the vertical. The main change observed when decreasing the grid spacing from 1.5 km to 100 m is that the highest-resolution models (200 and 100 m in this case) start to resolve turbulent motions in the boundary layer. This can be seen in Fig. 3, which shows the modification of the structure and enhancement in the strength of the convergence lines with decreasing grid spacing. Figure 4 shows the comparison between modeled vertical velocities and those measured by the BAe 146. The 1.5-km model crudely represents the main convergence line, whereas the 100-m model, qualitatively, looks much more like the observational data with numerous positive and negative spikes in vertical velocity as a result of boundary layer overturning.

Figure 5 shows parts of the convergence line on 5 July 2013 observed by the NCAS radar. The line is clearly visible in the radar reflectivity plot extending from south of the radar at 20-km range to east of the radar at 10-km range. It is less distinct, but nevertheless apparent in the Doppler velocity plot as a region of convergence about 10-km range from the radar from the south to the east. Air was moving toward the radar at 3–6 m s^{-1} within 10 km west to northwest (NW) of the radar and away from the radar within 10 km south to the east. The velocity changes to 0–2 m s^{-1} toward the radar at a range of 10 km. It is likely that the higher reflectivity at the location of the convergence line is due to the accumulation of insects in that region (e.g., Wilson et al. 1994).

OVERVIEW OF CONVECTIVE CLOUD CASES. Six cases of deep convection occurred during the COPE field campaign: 18, 28, and 29 July and 2, 3, and 5 August (Table 1). Four of those six included observations from both cloud physics aircraft and the NCAS radar; one included observations from the MOCCA. An additional five cases focused on warm clouds that were capped at or near the 0°C level, one of which included measurements from both aircraft. Two others were located outside of the main COPE study region and therefore lack ground-based radar measurements. An additional two IOPs focused on nocturnal mesoscale convective complexes (MCCs) and involved radar observations only.

Figure 6 shows two of the soundings from COPE IOPs, illustrating the range of environments sampled during the project. On 15 August (black lines), a region of elevated subsidence created significant drying and a strong cap that inhibited any deep convection, although the moist and convectively unstable atmosphere below this was conducive to widespread shallow convection. In contrast, 29 July (red lines) was considerably cooler, somewhat dryer in low levels, and lacked a strong lid allowing cloud tops to reach

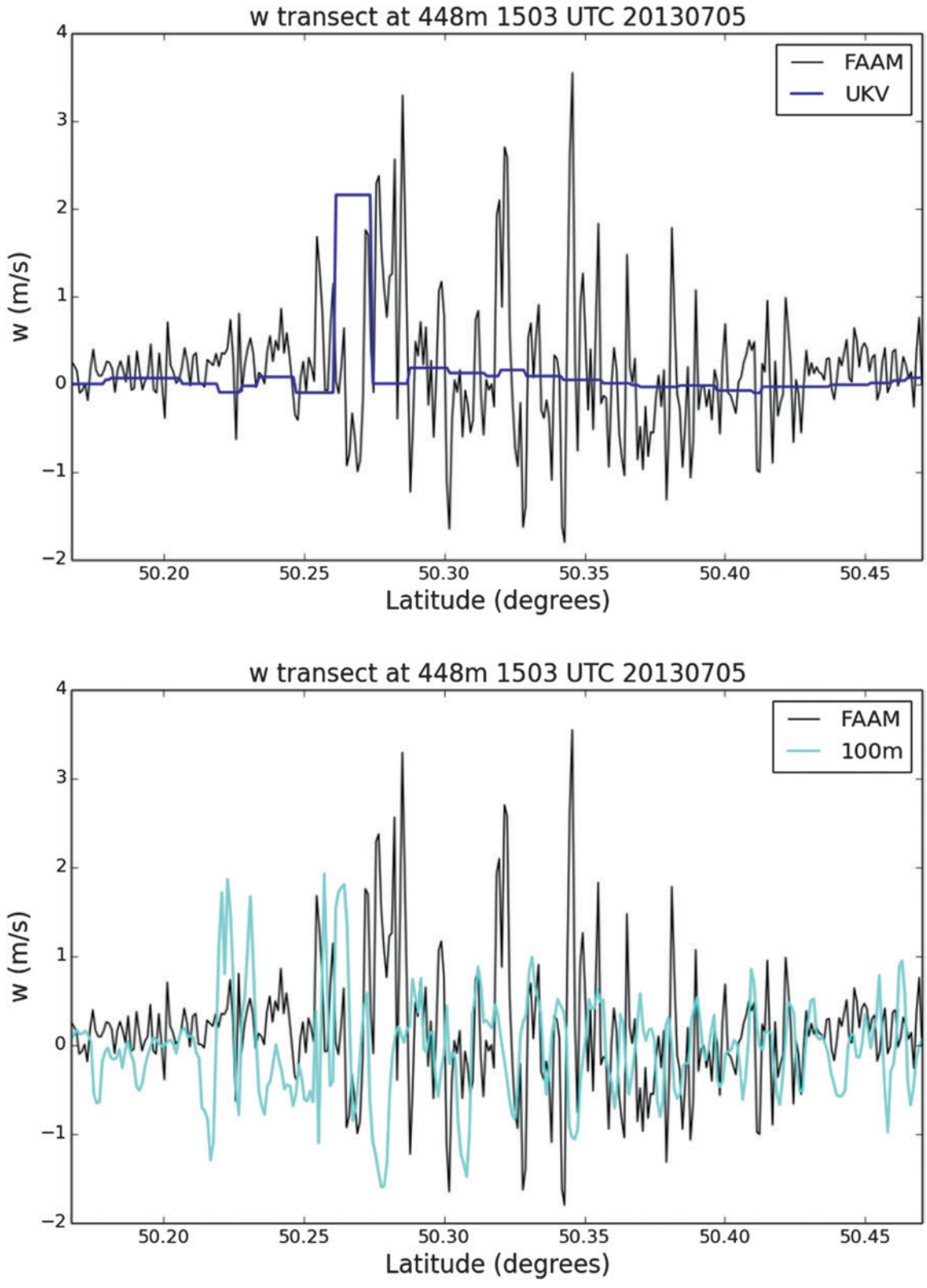

Fig. 4. Vertical velocity on aircraft transect across convergence line comparing observations with (top) UKV (1.5-km resolution) and (bottom) 100-m model. Location of transect corresponds to line A–B in (top left) of Fig. 3.

approximately −25°C. The convection on this day was less widespread but significantly deeper. Despite the different environments, and therefore vastly different contributions from warm rain versus ice processes, heavy rain was produced in both cases.

A wide range of microphysical conditions were sampled during COPE, as illustrated in Fig. 7. At times, a stable layer near the 0°C level (Fig. 6) limited vertical development of the cumuli. Warm rain formation on some days, such as 10 July, was likely limited by high aerosol concentrations resulting in cloud droplet concentrations in excess of 1,800 cm^{-3}. Only a few small raindrops were measured in these clouds. Other cases with lower droplet number concentrations were observed to have a vigorous warm rain process, such as on 15 August, where radar echoes greater than 50 dBZ were produced by clouds with tops that only extended to −3°C.

There was also substantial variability in the deeper clouds as indicated in Fig. 7: some clouds contained limited amounts of ice and graupel, seemingly dominated by the warm rain process at least through the −10° to −12°C level. On 2 August, for instance, there were strong updrafts and high liquid water contents and relatively low concentrations of particles with diameters greater than 100 μm (generally <20 L^{-1}), most of which were liquid or lightly rimed graupel (circular images). There were relatively few (<10%) columns. On the other hand, in cases such as 29 July, with similar cloud-base droplet concentrations and liquid water contents, but weaker updrafts, there was more graupel, ice, and evidence of an active Hallett–Mossop process, as indicated by a large number of columns (>90%) observed at temperatures greater than −10°C. Particles with diameters greater than 100 μm often occurred in concentrations of at least 100 L^{-1} with a greater percentage of irregular particles (typically heavily rimed graupel) and up to 40% columnar-type crystals.

The ratios of observed LWCs to adiabatic values (L_{obs}/L_{ad}) measured during COPE tended to be largest on days with the highest droplet concentrations, in excess of 1,000 cm^{-3}. On these days, observations of updraft cores

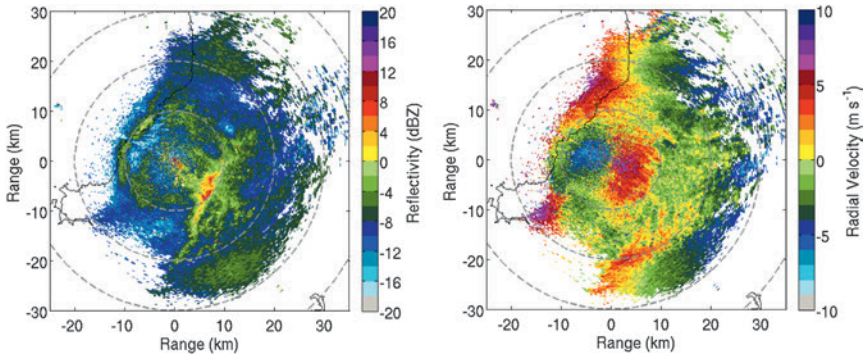

Fig. 5. NCAS (left) radar reflectivity and (right) radial Doppler velocity plan position indicator (PPI) at 1.5° elevation made at 1301 UTC 5 Jul 2013. The clear-air radar echoes are from insects in the boundary layer. The reflectivity and Doppler velocity scales are shown on the right of the respective diagrams, varying from −20 to +20 dBZ and −10 to +10 m s^{-1}, respectively. A region of convergence can be seen in the radial velocity plot at the boundary between the area of red and green at about 10-km range (approximately 250-m altitude).

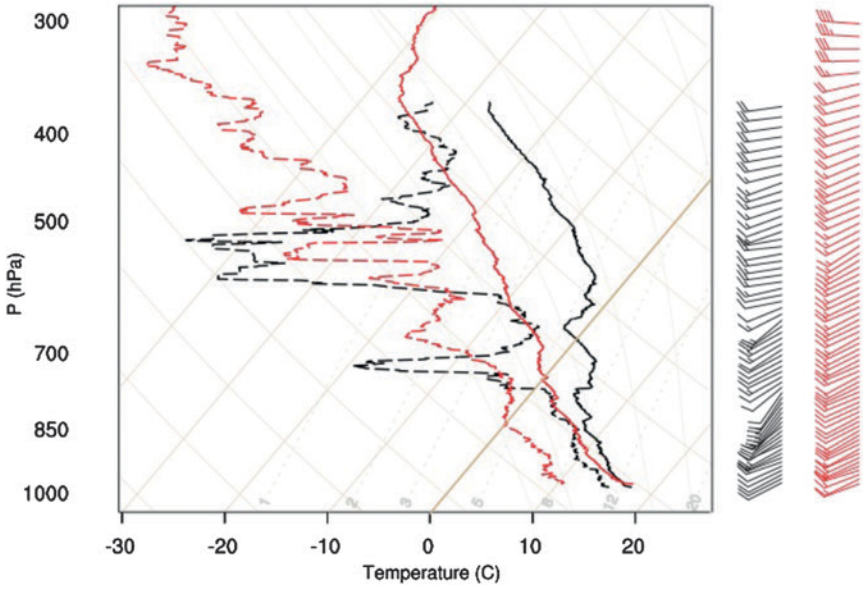

Fig. 6. Radiosonde data from the Cardington mobile sounding unit plotted on a skew *T*–log*p* diagram for 1300 UTC 29 Jul (red), where clouds grew substantially above the 0°C level, and 1200 UTC 15 Aug (black), where a strong stable layer limited cloud tops to near the 0°C level. Zero degree isotherm highlighted for clarity.

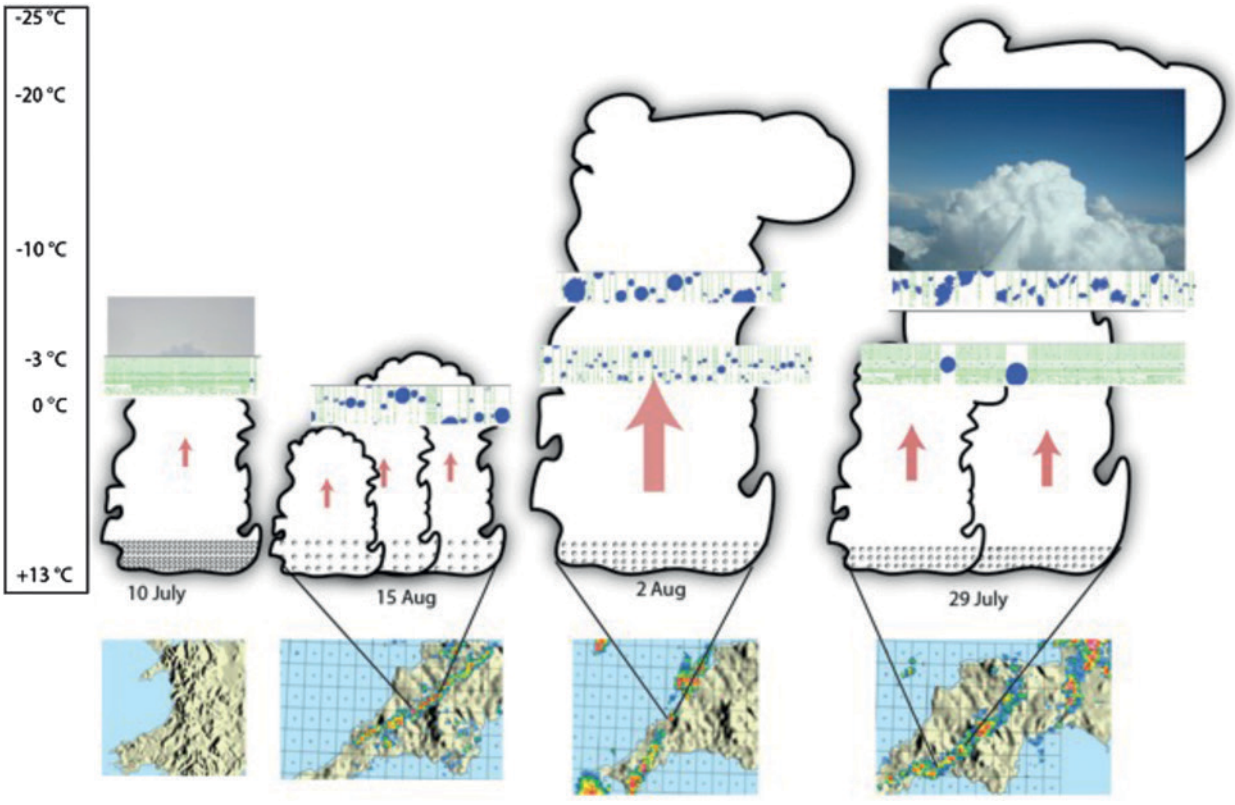

Fig. 7. Schematic illustration of key differences between COPE IOPs on 10 Jul, 15 Aug, 2 Aug, and 29 Jul. Both 15 Aug and 29 Jul consisted of tightly packed cells along a convective line, drawn as multiple clouds. Dot spacing near cloud bases is proportional to measured cloud droplet concentrations (1870, 240, 500, and 600 cm^{-3}, left to right). Size of arrows inside clouds is proportional to maximum updraft strength (5, 5, 18, and 10 m s^{-1}, respectively). Temperature scale on far left indicates approximate temperature of cloud bases and maximum cloud tops on each day. Samples of particle images from a cloud imaging probe (CIP) are displayed at the temperature where they were collected near ascending cloud tops. Radar images are composite rainfall from the UKMO radars; clouds sampled on 10 Jul over Wales did not precipitate. Pictures taken from the aircraft near cloud tops are shown for 10 and 29 Jul, indicative of hazy skies or the lack thereof.

100 m and wider contained mean LWCs in excess of 75% adiabatic values at 2.5–3.0 km above cloud base. Conversely, on days with significantly lower droplet concentrations, the ratios L_{obs}/L_{ad} generally were less. These days also showed a greater propensity to produce precipitation at levels 2–3 km above cloud base. So, the reduced LWCs on these days likely resulted from scavenging of cloud water by larger hydrometeors. Clouds on the high droplet concentration days were devoid of such scavenging and the observations clearly suggest the presence of cores reasonably well protected from entrainment and evaporation; however, little can be said at this time regarding the low droplet concentration days owing to the presumed reduction in LWC by precipitation scavenging.

THE IMPORTANCE OF THE WARM RAIN PROCESS. In a region notorious for persistent drizzle, one surprising result from COPE was the observation of heavy precipitation from the warm rain process alone. Radar reflectivity frequently in excess of 50 dBZ and occasionally exceeding 55 dBZ, sometimes accompanied by Z_{DR} up to 4 dB, was observed in clouds with tops constrained by a stable layer near the 0°C level resulting in a cloud depth of less than 2.5 km. Three such cases were sampled during COPE: 25 July and 14 and 15 August. The first is shown in Fig. 8. Comparable radar echoes (occasionally in excess of 60 dBZ) have been reported in Hawaiian rainbands (Szumowski et al. 1997, 1998) from similarly shallow clouds but with warmer cloud-base temperatures and lower droplet concentrations (around 20°C and 100 cm^{-3} or less, respectively) compared to those observed during COPE (around 14°C, and often in excess of 400 cm^{-3}, respectively). Further investigation into how cloud dynamics may help overcome conditions that appear significantly less favorable for warm rain production is underway.

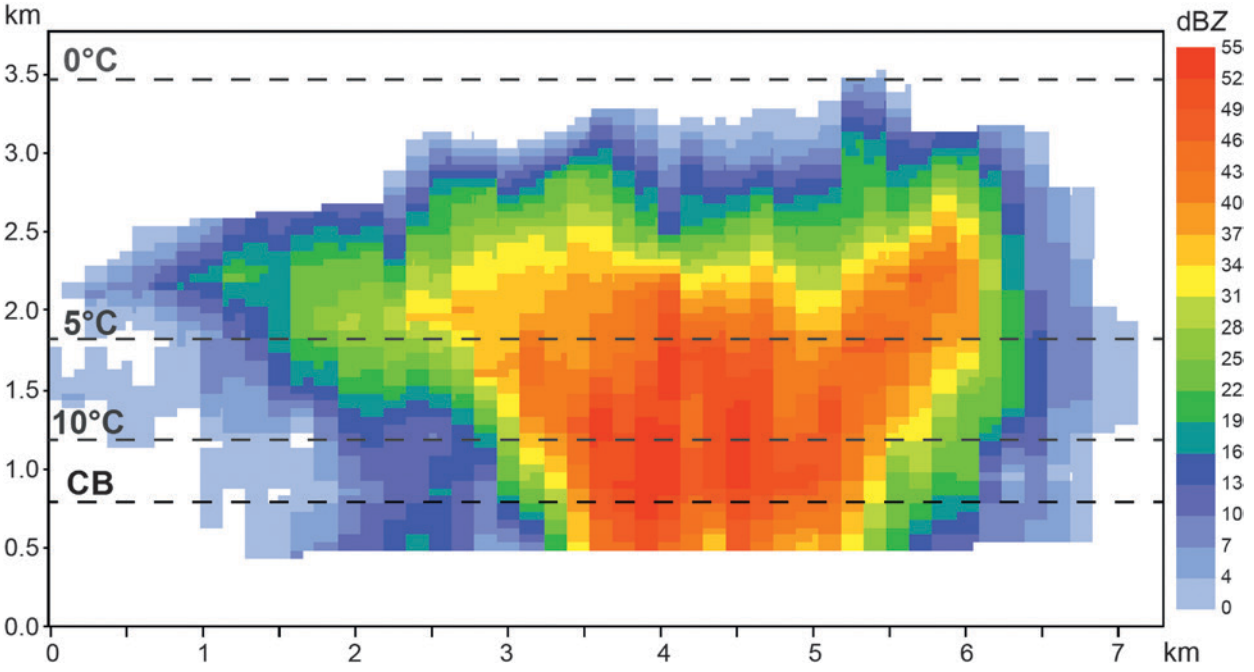

Fig. 8. Vertical cross section through the 1323 UTC NCAS radar volume scan on 25 Jul 2013. Bold line labeled "CB" denotes cloud-base height estimated from aircraft; dashed lines denote environmental isotherms as labeled. Cloud-base droplet number concentrations were in excess of 400 cm^{-3}.

POTENTIAL FLASH FLOOD CASE: 3 AUGUST 2013. Most of the ingredients needed to produce flash flooding, with the notable exception of heavy precipitation being concentrated within a suitable catchment, came together on 3 August 2013. Convergence lines triggered deep convection resulting in intense rainfall. Radar reflectivity in excess of 50 dB*Z*, reaching a maximum of nearly 60 dB*Z*, indicative of rainfall rates from about 50 mm h^{-1} to significantly in excess of 100 mm h^{-1}, was observed.[1]

UKV forecasts for 3 August predicted deep convection starting as early as 1200 UTC with well-defined convective lines along the spine of the peninsula by 1400 UTC. Based on these forecasts the BAe 146 took off at 1115 UTC followed by the UWKA at 1130. The BAe 146 sampled the boundary layer for 45 min while the UWKA sampled the first development of convection far to the southwest. By 1200 UTC, both aircraft were sampling convective clouds developing along a line that extended south of the NCAS radar.

A pair of stationary lines formed on 3 August 2013 with the more southerly of these lines eventually becoming dominant. Figure 9 shows a sequence of constant-altitude plan position indicators (CAPPIs) from the NCAS radar for the period when rainfall was most intense. The plots for each approximately 5-min scan are displaced in order to show the changes in the characteristics of the convective line. There was significant temporal and spatial variability in the reflectivity as cells within the line formed and decayed over a period of about 30 min. Clouds were closely packed along the line as evident in Fig. 10. Reflectivity exceeding 50 dB*Z* was associated with some clouds whose tops remained below the 0°C level. There was evidence of multiple thermals where new cells formed in the vicinity of decaying cells, which may have important implications for microphysical processes due to the incorporation of ice from older cells into newly developing turrets.

The line of convection was also broad with considerable nonlinear structure within the higher reflectivity regions. New development of cells did occur on the SW side, but new cells also formed along the line, often on the northwest and southeast sides. The cells developed relatively quickly as can be seen by examining the evolution of the new cell at the most southerly point from 1422 to 1436 UTC. The reflectivity in this cell increased from about 25 to 45 dB*Z* over 14 min. Radar-derived precipitation rates for these cells will be compared with model rates in future work.

During the penetration shown in Fig. 11 (1248:12–1248:42 UTC) at the –8°C level, the UWKA measured a region of 4 to 9 m s^{-1} updraft in the center of cloud with weak downdraft of –2 to –4 m s^{-1} nearer to the

[1] Rain rates computed using $Z = 200R^{1.6}$ following Harrison et al. (2012).

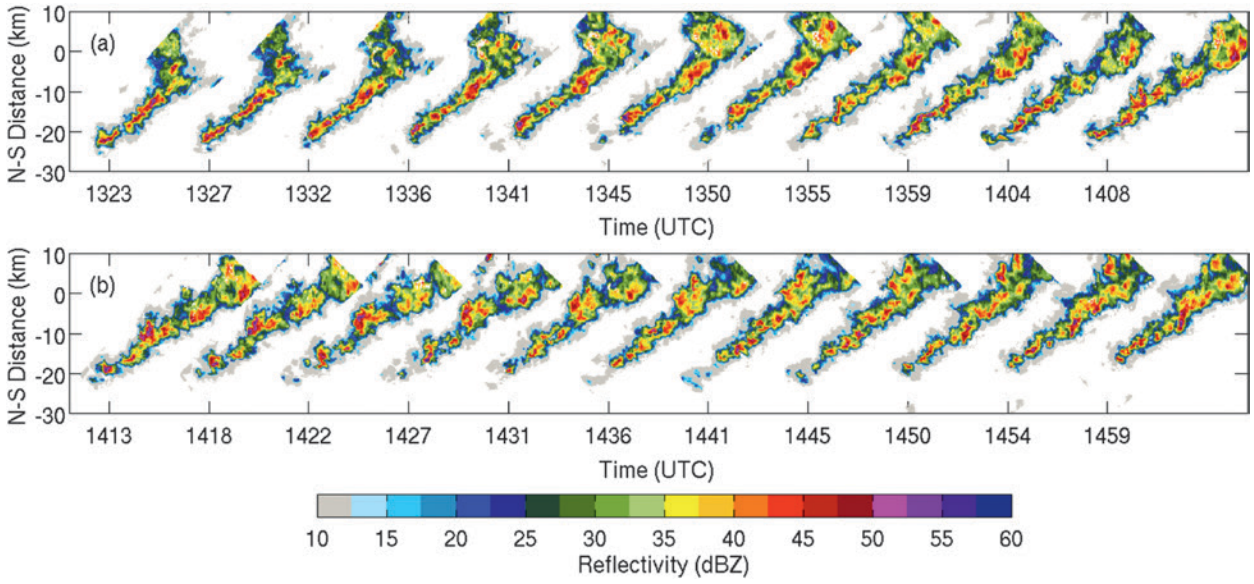

Fig. 9. Time sequence of NCAS radar constant-elevation reflectivity plots from (a) 1323 to 1408 UTC and (b) 1413 to 1459 UTC 3 Aug 2013. The SW end of the line was approximately 20 km south of the radar.

cloud edges. The traces of the LWC and cloud droplet concentration (not shown) had a "top hat"-type structure and, interestingly, the lowest LWC was sampled near the center of cloud, near the largest updraft. The depletion of liquid water in this location was likely due to cloud droplet scavenging by larger precipitation particles. Even though concentrations of precipitation-sized hydrometeors (defined here as $D > 100\ \mu$m) were less than near cloud edges, the particles themselves were significantly larger. These larger particles, classified as "spheres," deviated from purely spherical and were likely large graupel. A higher-resolution imaging probe also indicated an increase in the percentage of needlelike images in this region—indicating this is likely a region of secondary ice production. However, owing to probe resolution, only particles larger than about 125 μm may be classified so little can be said about the number of ice crystals smaller than this. Nearer to the cloud edges, precipitation particle concentrations are more than an order of magnitude greater; however, the mean diameter of these particles is smaller by a factor of 2, and the volume-weighted mean diameter is smaller by a factor of 5.

During the penetration shown in Fig. 12 (1343:35–1344:05 UTC) at the –12°C level, the UWKA encountered a broad updraft of 4 to 9 m s^{-1} on the upwind side of the cloud and an equally broad downdraft of –5 to –10 m s^{-1} on the downwind side. At these higher altitudes and lower temperatures, much of the LWC had been consumed by the precipitation. The strongest updraft contained LWC up to 1.5 g m^{-3}, but the transition zone (region B) was devoid of cloud liquid.

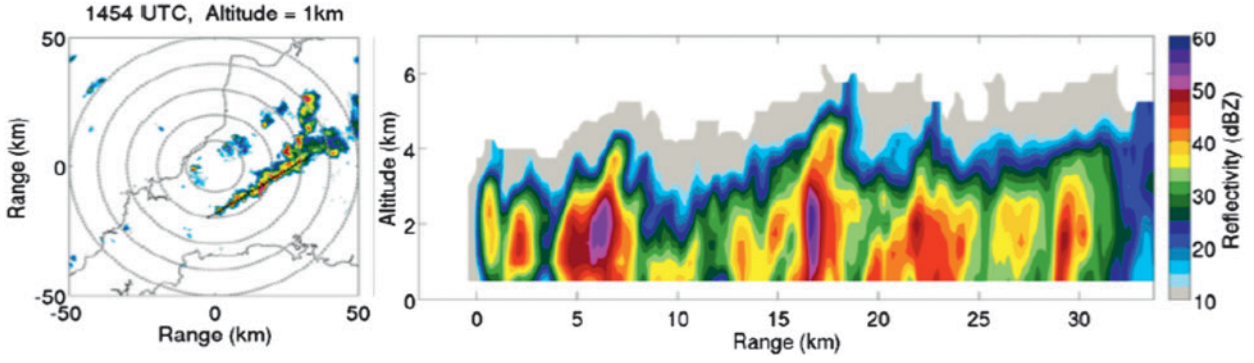

Fig. 10. (left) PPI from NCAS radar. Dotted line indicates location of cross section [shown in (right)]. Note weaker echoes along more northerly convergence line. (right) Cross section along the line showing the closely packed nature of the cells.

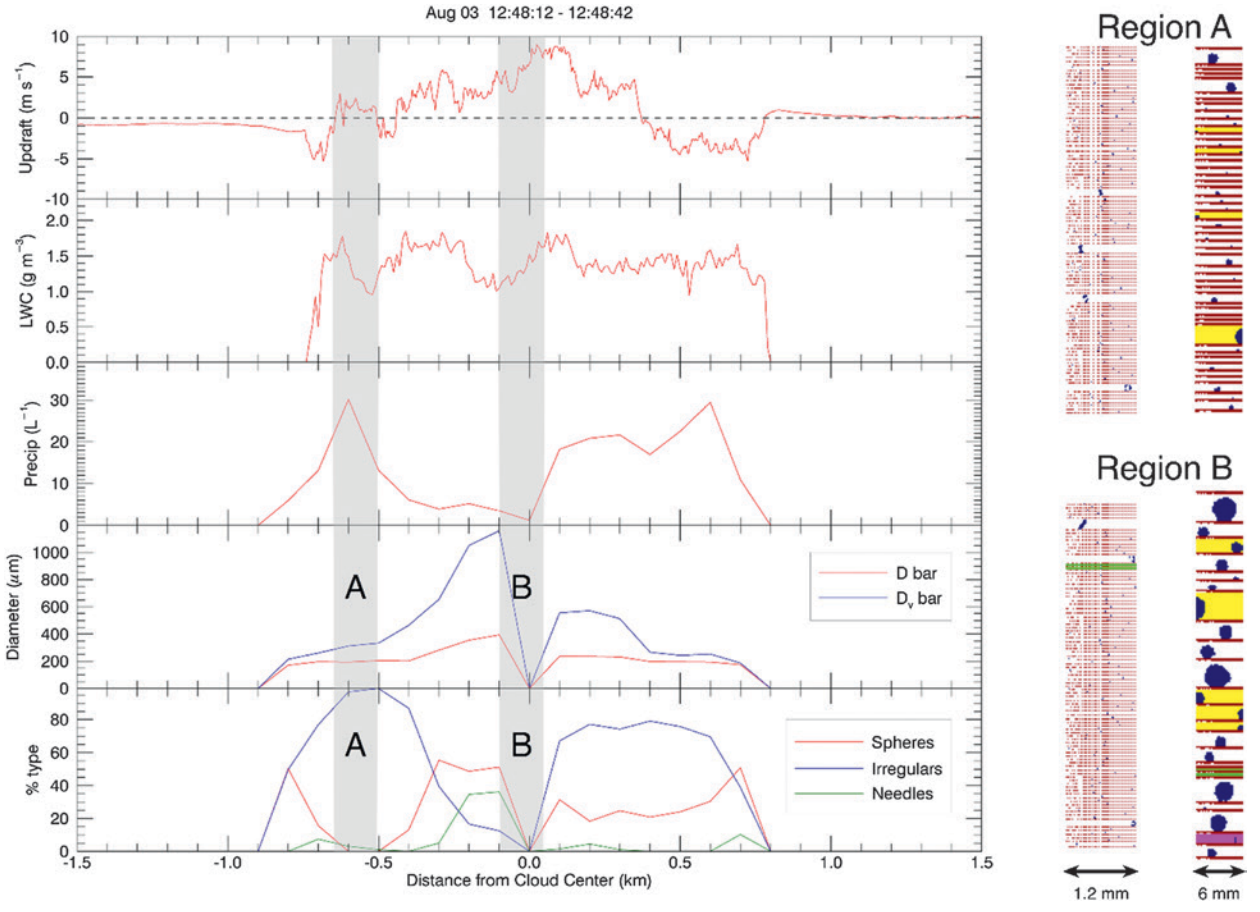

Fig. 11. Trace of select variables measured by the UWKA during a penetration at –8°C on 3 Aug 2013. (from top to bottom) Vertical winds, cloud liquid water content, hydrometeor concentration of particles with diameter greater than 100 μm (precipitation; see text), mean diameter and mean volume diameter of precipitation, and percent of precipitation particles classified as spheres, irregulars, or needles. (right) Sample images from the OAP CIP and 2DP OAP are shown for two ~150-m-wide regions defined by the shaded boxes in the trace. At the bottom right, a size scale is shown for the sample buffer size.

Precipitation particles in that region were mostly irregular, but there was also a significant portion of them that were classified as needlelike—mostly the smaller 100–200-μm crystals. Farther downwind, in the downdraft (region A), nearly all precipitation hydrometeors were classified as irregular. Images from the OAPs indicate heavily rimed crystals, and a few (not shown) appear to have undergone significant growth through diffusion (having a platelike appearance).

PROMISING AREAS FOR FOLLOW-UP AND FUTURE RESEARCH. Prior to COPE, there had never been a field campaign to measure the microphysics and dynamics of the convective clouds in the southwest of England. It is a region prone to flash flooding owing in part to sea-breeze convergence lines resulting from the shape of the peninsula, solar heating, and the direction of the prevailing winds. The 17 cases observed during the project constitute a unique dataset with which to test NWP models. The biggest surprise of the COPE field campaign was the large reflectivity values (exceeding 50 dBZ) in shallow convection and the observation of large raindrops. It is an opportunity for understanding the development of rain by collision and coalescence and addressing questions regarding the importance of entrainment, turbulence, and ultragiant nuclei. The variety of aerosol concentrations and consequent cloud droplets add to this opportunity. The two cases that will be studied in most detail, however, are 2 and 3 August, where strong convergence lines developed with similar, but significantly different, characteristics to the 2004 Boscastle flood (Golding et al. 2005). The initiation and evolution of ice particles and in particular the role of dynamics in the operation of the Hallett–Mossop process will be examined in these two and other cases, where clouds ascended beyond local stable layers allowing ice particles and significant precipitation to form.

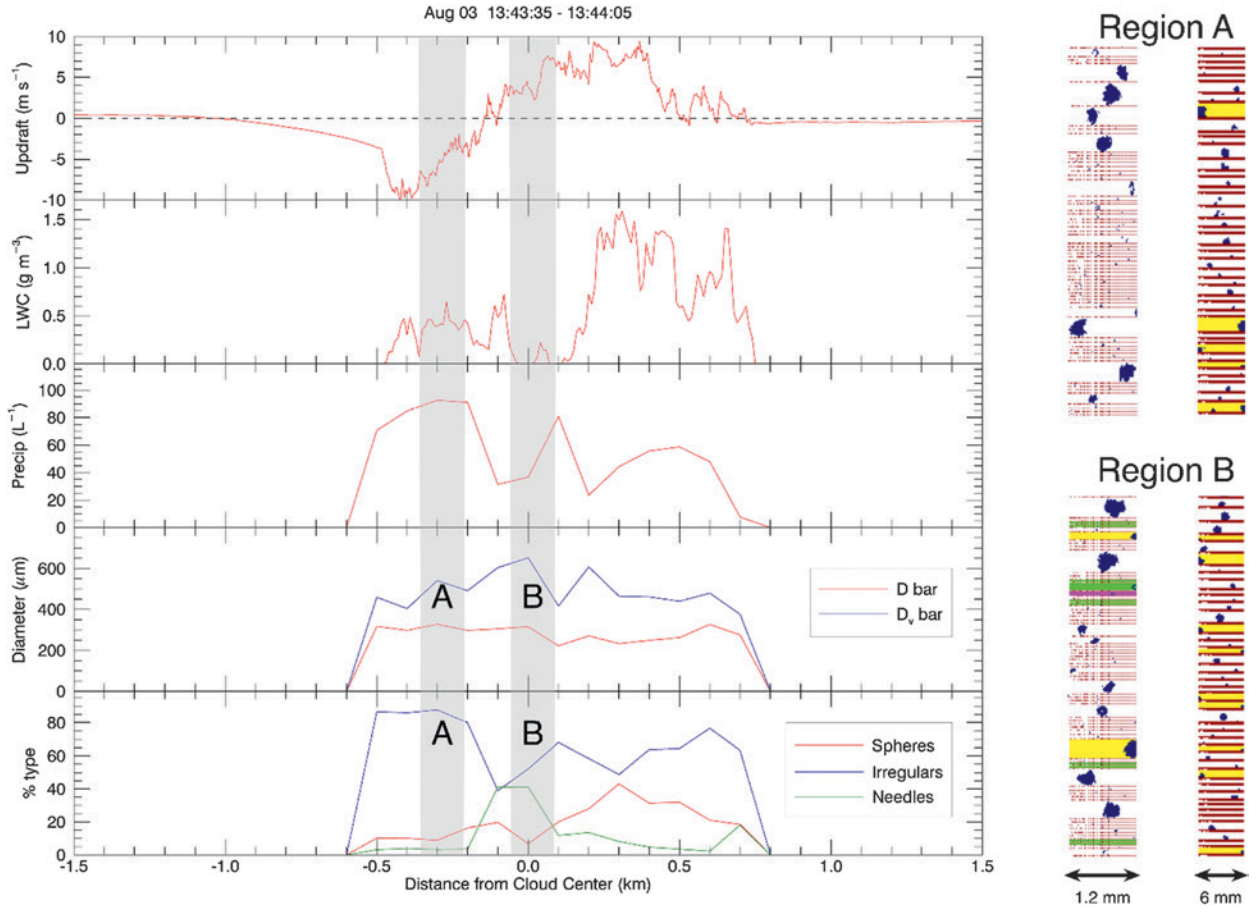

Fig. 12. As in Fig. 11, but for a penetration in a separate cloud at –12°C on 3 Aug 2013.

Continuing study of these cases and others is important to understand how the models at various resolutions represent convection and microphysical processes. The main change observed when increasing the resolution of the models is that the representation of the convergence line improves (Fig. 13), with the 200-m simulation able to capture the double line structure. This is in agreement with initial work looking at the resolution dependence of peninsula convection undertaken by Warren et al. (2014), who found an improved representation of convergence lines when moving from 1.5-km to 500-m grid spacing. Another improvement seen when increasing the resolution is in the shape of the convective cells, with cells in the UKV and even the 500-m simulations being too smooth and circular. An important aspect of this work is to improve the

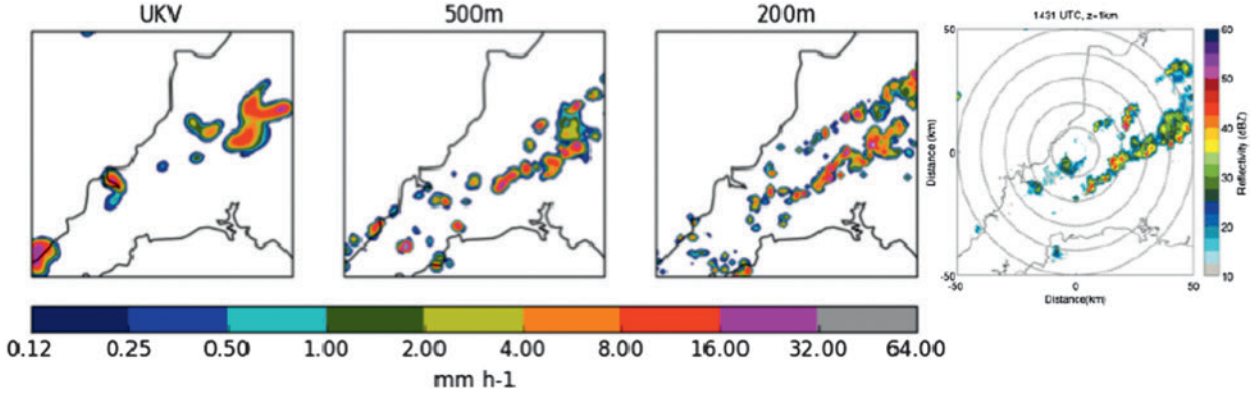

Fig. 13. (left three panels) Surface rain rate (mm h^{-1}) from models at different resolutions compared with (right) reflectivity from the NCAS radar (in dBZ) at 1430 UTC 3 Aug 2013.

representation of microphysical processes in subkilometer grid spacing models. The COPE dataset will be invaluable for testing these and other models at different resolutions and to guide these improvements.

ACKNOWLEDGMENTS. This work was partly funded by NERC under the auspices of Grant NE/J023507/1. The U.S. investigators were funded by NSF Grants AGS-1230292 and AGS-1230203. The Met Office funded the operation of the BAe 146 FAAM aircraft, which is owned by NERC and operated jointly by NCAS on behalf of NERC and the Met Office. NSF (AGS-1441831) funded the participation of the UWKA. We would like to acknowledge BADC for storing archived COPE data and NCAS AMF for use of the mobile dual-polarization radar, the wind profiler, Doppler lidar, rain radar, and AWS systems. Excellent logistical support was provided by several people at Davidstow, United Kingdom—in particular, Steve and Sheila Perry and Martin Kent at Davidstow Airfield and Cornwall at War Museum, Julie Dowton, and personnel at DairyCrest Ltd. for which we are very grateful. We would also like to thank Colin Tully and Emily Evans for their help and support with the NCAS radar.

REFERENCES

Allen, G., and Coauthors, 2011: South East Pacific atmospheric composition and variability sampled along 20°S during VOCALS-REx. *Atmos. Chem. Phys.*, **11**, 5237–5262, doi:10.5194/acp-11-5237-2011.

Beard, K. V., D. B. Johnson, and D. Baumgardner, 1986: Aircraft observations of large raindrops in warm, shallow, convective clouds. *Geophys. Res. Lett.*, **13**, 991–994, doi:10.1029/GL013i010p00991.

Bringi, V. N., L. Liu, P. C. Kennedy, V. Chandrasekar, and S. A. Rutledge, 1996: Dual multiparameter radar observations of intense convective storms: The 24 June 1992 case study. *Meteor. Atmos. Phys.*, **59**, 3–31, doi:10.1007/BF01031999.

——, K. Knupp, A. Detwiler, L. Liu, I. J. Caylor, and R. A. Black, 1997: Evolution of a Florida thunderstorm during the Convection and Precipitation/Electrification Experiment: The case of 9 August 1991. *Mon. Wea. Rev.*, **125**, 2131–2160, doi:10.1175/1520-0493(1997)125<2131:EOAFTD>2.0.CO;2.

Browning, K. A., and Coauthors, 2007: The Convective Storm Initiation Project. *Bull. Amer. Meteor. Soc.*, **88**, 1939–1955, doi:10.1175/BAMS-88-12-1939.

Caracena, F., R. A. Maddox, L. R. Hoxit, and C. F. Chappell, 1979: Mesoanalysis of the Big Thompson storm. *Mon. Wea. Rev.*, **107**, 1–17, doi:10.1175/1520-0493(1979)107<0001:MOTBTS>2.0.CO;2.

Clark, A. J., W. A. Gallus, M. Xue, and F. Kong, 2009: A comparison of precipitation forecast skill between small convection-allowing and large convection-parameterizing ensembles. *Wea. Forecasting*, **24**, 1121–1140, doi:10.1175/2009WAF2222222.1.

Clark, P., N. Roberts, H. Lean, S. P. Ballard, and C. Charlton-Perez, 2016: Convection-permitting models: A step-change in rainfall forecasting. *Meteor. Appl.*, doi:10.1002/met.1538, in press.

Cotton, R. J., and Coauthors, 2013: The effective density of small ice particles obtained from *in situ* aircraft observations of mid-latitude cirrus. *Quart. J. Roy. Meteor. Soc.*, **139**, 1923–1934, doi:10.1002/qj.2058.

Dey, S. R. A., G. Leoncini, N. M. Roberts, R. S. Plant, and S. Migliorini, 2014: A spatial view of ensemble spread in convection permitting ensembles. *Mon. Wea. Rev.*, **142**, 4091–4107, doi:10.1175/MWR-D-14-00172.1.

Duda, J. D., X. Wang, F. Kong, and M. Xue, 2014: Using varied microphysics to account for uncertainty in warm-season QPF in a convection-allowing ensemble. *Mon. Wea. Rev.*, **142**, 2198–2219, doi:10.1175/MWR-D-13-00297.1.

Fritsch, J. M., and R. E. Carbone, 2004: Improving quantitative precipitation forecasts in the warm season: A USWRP research and development strategy. *Bull. Amer. Meteor. Soc.*, **85**, 955–965, doi:10.1175/BAMS-85-7-955.

Golding, B. W., P. Clark, and B. May, 2005: Boscastle flood: Meteorological analysis of the conditions leading to flooding on 16 August 2004. *Weather*, **60**, 230–235, doi:10.1256/wea.71.05.

——, and Coauthors, 2014: Forecasting capabilities for the London 2012 Olympics. *Bull. Amer. Meteor. Soc.*, **95**, 883–896, doi:10.1175/BAMS-D-13-00102.1.

Hanley, K. E., R. S. Plant, T. H. M. Stein, R. J. Hogan, J. C. Nicol, H. W. Lean, C. Halliwell, and P. A. Clark, 2015: Mixing-length controls on high-resolution simulations of convective storms. *Quart. J. Roy. Meteor. Soc.*, **141**, 272–284, doi:10.1002/qj.2356.

Harrison, D. L., K. Norman, C. Pierce, and N. Gaussiat, 2012: Radar products for hydrological applications in the UK. *Proc. Inst. Civ. Eng.: Water Manage.,* **165**, 89–103, doi:10.1680/wama.2012.165.2.89.

Hobbs, P. V., and A. L. Rangno, 2004: Super-larger raindrops. *Geophys. Res. Lett.*, **31**, L13102, doi:10.1029/2004GL020167.

Houze, R. A., 1977: Structure and dynamics of a tropical squall-line system. *Mon. Wea. Rev.*, **105**, 1540–1567, doi:10.1175/1520-0493(1977)105<1540:SADOAT>2.0.CO;2.

Jameson, A., M. Murphy, and E. Krider, 1996: Multiple-parameter radar observations of isolated Florida thunderstorms during the onset of electrification.

J. Appl. Meteor., **35**, 343–354, doi:10.1175/1520-0450(1996)035<0343:MPROOI>2.0.CO;2.

Koenig, L., 1963: The glaciating behavior of small cumulonimbus clouds. *J. Atmos. Sci.*, **20**, 29–47, doi:10.1175/1520-0469(1963)020<0029:TGBOSC>2.0.CO;2.

Kumar, A., R. A. Houze, K. L. Rasmussen, and C. Peters-Lidard, 2014: Simulation of a flash flooding storm at the steep edge of the Himalayas. *J. Hydrometeor.*, **15**, 212–228, doi:10.1175/JHM-D-12-0155.1.

Kumjian, M. R., and A. V. Ryzhkov, 2008: Polarimetric signatures in supercell thunderstorms. *J. Appl. Meteor. Climatol.*, **47**, 1940–1961, doi:10.1175/2007JAMC1874.1.

Lean, H. W., N. M. Roberts, P. A. Clark, and C. Morcrette, 2009: The surprising role of orography in the initiation of an isolated thunderstorm in southern England. *Mon. Wea. Rev.*, **137**, 3026–3046, doi:10.1175/2009MWR2743.1.

Lhermitte, R., 1990: Attenuation and scattering of millimeter wavelength radiation by clouds and precipitation. *J. Atmos. Oceanic Technol.*, **7**, 464–479, doi:10.1175/1520-0426(1990)007<0464:AASOMW>2.0.CO;2.

Morcrette, C., H. Lean, K. Browning, J. Nicol, N. Roberts, P. Clark, A. Russell, and A. Blyth, 2007: Combination of mesoscale and synoptic mechanisms for triggering an isolated thunderstorm: Observational case study of CSIP IOP 1. *Mon. Wea. Rev.*, **135**, 3728–3749, doi:10.1175/2007MWR2067.1.

Petersen, G. N., and I. A. Renfrew, 2009: Aircraft-based observations of air–sea fluxes over Denmark Strait and the Irminger Sea during high wind speed conditions. *Quart. J. Roy. Meteor. Soc.*, **135**, 2030–2045, doi:10.1002/qj.355.

Petersen, W. A., and Coauthors, 1999: Mesoscale and radar observations of the Fort Collins flash flood of 28 July 1997. *Bull. Amer. Meteor. Soc.*, **80**, 191–216, doi:10.1175/1520-0477(1999)080<0191:MAROOT>2.0.CO;2.

Pontrelli, M. D., G. Bryan, and J. M. Fritsch, 1999: The Madison County, Virginia, flash flood of 27 June 1995. *Wea. Forecasting*, **14**, 384–404, doi:10.1175/1520-0434(1999)014<0384:TMCVFF>2.0.CO;2.

Rodi, A., 2011: King of the air: The evolution and capabilities of Wyoming's observations aircraft. *Meteorological Technology International*, May 2011, UKIP, Dorking, United Kingdom, 44–47.

Roberts, N., and H. Lean, 2008: Scale-selective verification of rainfall accumulations from high-resolution forecasts of convective events. *Mon. Wea. Rev.*, **136**, 78–97, doi:10.1175/2007MWR2123.1.

Rogers, R., 1967: Doppler radar investigation of Hawaiian rain. *Tellus*, **19**, 432–454, doi:10.1111/j.2153-3490.1967.tb01498.x.

Stein, T. H. M., R. J. Hogan, P. A. Clark, C. E. Halliwell, K. E. Hanley, H. W. Lean, J. C. Nicol, and R. S. Plant, 2015: The DYMECS project: A statistical approach for the evaluation of storms in high-resolution NWP models. *Bull. Amer. Meteor. Soc.*, **96**, 939–951, doi:10.1175/BAMS-D-13-00279.1.

Szumowski, M. J., R. M. Rauber, H. T. Ochs III, and L. J. Miller, 1997: The microphysical structure and evolution of Hawaiian rainband clouds. Part I: Radar observations of rainbands containing high reflectivity cores. *J. Atmos. Sci.*, **54**, 369–385, doi:10.1175/1520-0469(1997)054<0369:TMSAEO>2.0.CO;2.

——, ——, ——, and K. V. Beard, 1998: The microphysical structure and evolution of Hawaiian rainband clouds. Part II: Aircraft measurements within rainbands containing high reflectivity cores. *J. Atmos. Sci.*, **55**, 208–226, doi:10.1175/1520-0469(1998)055<0208:TMSAEO>2.0.CO;2.

Tang, Y., H. W. Lean, and J. Bornemann, 2013: The benefits of the Met Office variable resolution NWP model for forecasting convection. *Meteor. Appl.*, **20**, 417–426, doi:10.1002/met.1300.

Wang, Z., and Coauthors, 2012: Single aircraft integration of remote sensing and in situ sampling for the study of cloud microphysics and dynamics. *Bull. Amer. Meteor. Soc.*, **93**, 653–668, doi:10.1175/BAMS-D-11-00044.1.

Warren, R. A., D. J. Kirshbaum, R. S. Plant, and H. W. Lean, 2014: A 'Boscastle-type' quasi-stationary convective system over the UK Southwest Peninsula. *Quart. J. Roy. Meteor. Soc.*, **140**, 240–257, doi:10.1002/qj.2124.

Weckwerth, T. M., and Coauthors, 2004: An overview of the International H_2O Project (IHOP_2002) and some preliminary highlights. *Bull. Amer. Meteor. Soc.*, **85**, 253–277, doi:10.1175/BAMS-85-2-253.

Wilson, J. W., T. M. Weckwerth, J. Vivekanandan, R. M. Wakimoto, and R. W. Russell, 1994: Boundary layer clear-air radar echoes: Origin of echoes and accuracy of derived winds. *J. Atmos. Oceanic Technol.*, **11**, 1184–1206, doi:10.1175/1520-0426(1994)011<1184:BLCARE>2.0.CO;2.

Wulfmeyer, V., and Coauthors, 2011: The Convective and Orographically-induced Precipitation Study (COPS): The scientific strategy, the field phase, and research highlights. *Quart. J. Roy. Meteor. Soc.*, **137**, 3–30, doi:10.1002/qj.752.